Correlation of hierarchical porosity in nanoporous gold with the mass transport of electron transfer-coupled-chemical reactions

Abhishek Kumar, Mathieu F Bettinger, Vaibhav Vibhu, Marcel Bouvet, Rita Meunier-Prest

Graphical abstract

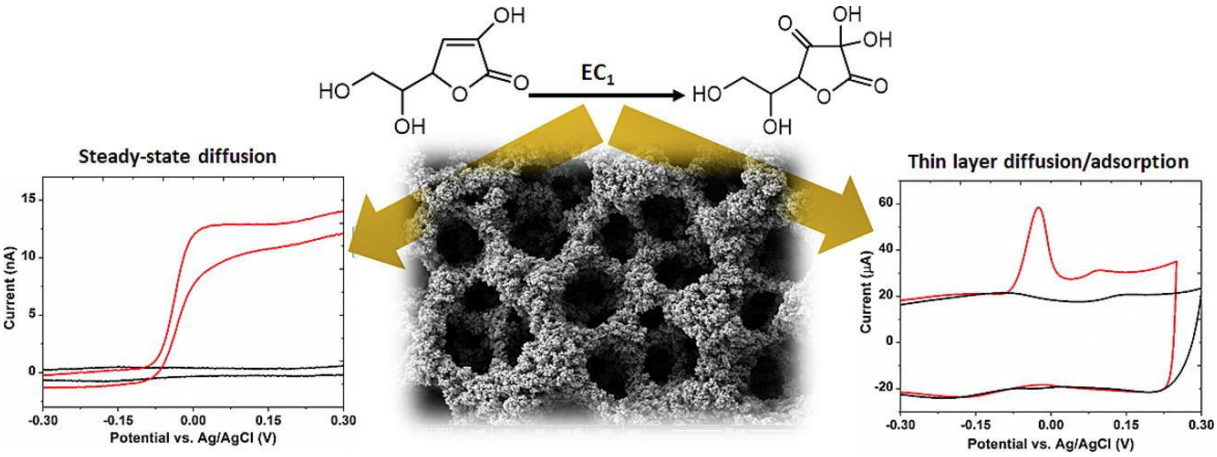

Correlation of hierarchical porosity in nanoporous gold with the mass transport of electron transfer-coupled-chemical reactions

Abhishek Kumar[1]*, Mathieu F. Bettinger[1], Vaibhav Vibhu[2], Marcel Bouvet[1], Rita Meunier-Prest[1]*

[1]*Institut de Chimie Moléculaire de l'Université de Bourgogne, UMR CNRS 6302, Université Bourgogne Franche-Comté, 9 Avenue Alain Savary, Dijon Cedex 21078, France*

[2]*Institute of Energy and Climate Research, Fundamental Electrochemistry (IEK-9), Forschungszentrum Jülich GmbH, 52425 Jülich, Germany*

Email addresses and ORCID number of authors (corresponding authors emails are marked with asterisk)

*abhishek.Kumar@u-bourgogne.fr (ORCID no. 0000-0002-4306-9644)

mathieu.bettinger@outlook.fr

v.vibhu@fz-juelich.de (ORCID no. 0000-0001-9157-2722)

marcel.bouvet@u-bourgogne.fr (ORCID no. 0000-0002-2272-6633)

*rita.Meunier-Prest@u-bourgogne.fr (ORCID no. 0000-0001-5597-3879)

Abstract: Optimization of mass transfer within a porous material is a highly promising strategy to improve the efficiency of electrode reactions. Herein, nanoporous gold (NPG) modified gold electrode is investigated to study the mass transport of ascorbic acid (AA), which oxidation process is characterized by an electrochemical coupled 1st order chemical reaction, commonly termed as EC_1 reaction. The template-assisted synthesis of NPG results into the formation of a highly pure and porous film of gold. However, the surface porosity of NPG depends on the choice of electrodeposition parameters, such as deposition time (t_d) and potential (E_d) and the size of the substrate. Such porosity variation of NPG strongly influences the voltammetric profile of AA anodic reaction, displaying sigmoidal, non-symmetric and symmetric peak features. The analysis of mass transport behaviour of AA reveals a combination of diffusion and thin layer EC_1 mechanism, predominance of which is determined by the E_d and t_d selected for NPG synthesis, as well as the size of the Au substrate. The mass transport of AA on NPG prepared on Au microelectrodes experienced a significant diffusion from bulk solution, owing to the larger pores, which permits the easier exchange of redox species between the NPG volume and the bulk solution. On the contrary, mass transport of AA on NPG deposited on big Au electrode has a significant contribution of thin layer diffusion, attributed to the smaller surface pores of NPG, which limits the exchange of AA and its oxidized form from the bulk solution.

Keywords: Nanoporous metal, Mass transport, EC reactions, Electrocatalysis, Ascorbic acid

1. Introduction

Nanoporous metal has attracted profound research interests in diverse research areas, such as electrochemical energy conversion and storage [1, 2], electrocatalysis of important chemical reactions [3] and electrochemical sensors [4-6]. Conventionally, the research interests in such materials were mainly driven by their large surface to volume ratio, expected to provide enlarged area for the electrochemical reactions. However, with the advancement of fundamental researches in this domain, the importance of crystalline facets and unique nanoporous geometry have been realized, which mainly determine the selectivity and the kinetics of the reactions [7-10]. Moreover, with the understanding of nanoporous electrochemistry and the nature of interfaces in the nanoporous confined environment, the unique ionic and molecular transport phenomena were revealed [11], which further expanded the applications of these materials in selective membranes and ionotronics devices [12]. The common structural architecture of these materials is characterized by the interconnected network of nanometric struts and pores, which may be bicontinuous or unidirectional, depending on the choice of synthetic method. In one approach, these materials are synthesized by chemical/electrochemical dealloying of a binary/ternary alloy, which results in selective dissolution of the less noble metal/metals, creating an empty space in the microstructure [13, 14]. In another approach, synthesis is based on template-assisted electrodeposition [15], such as dynamic hydrogen bubble deposition (DHBT), in which the evolution of hydrogen bubbles provides a template to metal deposit, thus generating porosity in the metal film [16]. The choice of a synthetic method and control of the synthesis parameters impart wide variations in the porous morphology and the microstructure of these materials, which strongly influence the kinetics of electrode reactions.

Majority of the electrode reactions relevant in practical applications are coupled processes, involving electrochemical and chemical reactions. They are commonly termed as

EC or CE processes, depending on if chemical step follows or precedes the electrochemical step, respectively. The oxidation process of ascorbic acid (AA) is a classic example of coupled EC reactions, involving an electrochemical step followed by a fast 1st order chemical reaction [17]. Investigation of AA oxidation process and monitoring of its concentration in biofluid have drawn a lot of interests from researchers [18], owing to its important role in cellular redox metabolism [19] and its widespread use in food and pharmaceutical industries as an antioxidant [20]. Conventionally, electroanalysis of AA was mainly performed on unmodified metal [21] and carbon electrodes [22], using different voltammetric techniques. However, the voltammetric response of AA on unmodified electrodes is low, exhibits higher overpotential and is interfered by dopamine (DA) and uric acid (UA), which usually coexist with AA in the real samples, such as biofluid. Moreover, oxidation product of AA, dehydroascorbic acid (DHA) strongly adsorbs on the unmodified electrodes, making them inaccessible for the further electrochemical events. These limitations have been overcome in recent years through modification of the conventional electrodes with host of electrocatalytic nanomaterials [23], such as metal nanoparticles [24], carbon-based nanomaterials [25] and nanoporous metals. Out of these nanomaterials, nanoporous metal-based electrode modifiers have clearly stood out, owing to the high electrochemical activity towards AA, large surface area and their facile synthesis on the electrode surface. We reported recently DHBT grown nanoporous gold (NPG) modified gold electrode, as highly sensitive and selective electroanalytical platform for the detection of AA in neutral and acidic medium [26-28]. Elsewhere, NPG prepared by chemical dealloying was used as an electrode modifier for voltammetric and potentiometric detection of AA in biofouling conditions [29-31]. Other than NPG, gold and platinum containing nanoporous alloys were also electrosynthesized for selective electrochemical detection of AA in the presence of DA and UA [32-34]. Despite highly promising electrocatalyic properties of

nanoporous metal in AA oxidation process, the mass transport limitation in the nanoporous volume remains a pertaining challenge to overcome.

The mass transport dynamics of the redox species and the ions inside the complex nanoporous structure are very different from the bulk solution and those observed at the plane electrode-solution interface. The larger pores facilitate the effective mass transport within the porous volume but come at the cost of offsetting the available surface area for the faradaic process. On the other hand, smaller pores can provide enlarged surface area but it also impedes the mass transport of larger redox species and ions within the confined nanochannels. Therefore, an appropriate nanoporous electrode design is required to optimize the mass transport of the redox and the electrolyte species. Moreover, the size of the pores must be larger than the thickness of Electric Double Layer (EDL), otherwise EDL overlapping occurs, making the pores inaccessible for the redox species and the ions [35]. Besides the porous geometry of nanoporous metal, the kinetics of the EC reactions also influence the transport dynamics within the electrode volume. Accordingly, redox species undergoing sluggish electrochemical reactions can travel deeper into the porous volume and access the larger area, while those showing faster electron transfer reactions can deplete immediately after entering the pores and do not benefit from the large area effect [36]. Therefore, an intricate optimization of porous morphology is necessary to design a nanoporous catalyst, which must be commensurate with the kinetics of the targeted electrochemical processes. Such studies remain in infancy for the EC reactions of AA on NPG modified electrode. Recently, we reported mass transport studies of AA on NPG modified gold microelectrode [37]. However, mass transport evaluation of AA on NPG electrodeposited on different sizes of electrode, in particular an intercomparison between microelectrode and millimeter-sized electrode, has not been yet performed. It is worth noting that surface pores of the NPG prepared by DHBT method on microelectrode and on millimeter-sized electrode can be very different, owing to the different transport regimes. Thus,

surface pores evolution of NPG on different sizes electrodes should be systematically assessed and correlated to mass transport of AA electrode processes.

In this endeavor, the present work investigates the mass transport of AA oxidation process on NPG film, electrodeposited at different sizes of gold electrode, which are further correlated to the surface pores of the NPG. The NPG films are extensively characterized by cyclic voltammetry (CV), scanning electron microscopy (SEM) and X-ray photoelectron spectroscopy (XPS) to assess their surface area, morphology and chemical purity, respectively. The electrochemical activity of AA on different NPG modified gold electrodes has been studied by CV, performed in a wide range of AA concentration and of the scan rate. Finally, the voltammetric profiles of AA oxidation process are comprehensively analyzed and mass transport behavior is evaluated on different NPG coated Au electrodes.

2. Experimental

2.1. Materials and reagents

Analytical grade chemicals were used in this work as received from the seller. Gold(III) chloride trihydrate ($HAuCl_4 \cdot 3H_2O$, Molecular weight: 393.83 g mol^{-1}), L-ascorbic acid ($C_6H_8O_6$, Molecular weight: 176.12 g mol^{-1}) and phosphate buffer saline (PBS) tablets were procured from Sigma-Aldrich. The hard gold fibers of diameter 25 µm, 50 µm and 100 µm were purchased from Goodfellow, UK. The gold disk electrode of diameter 1.6 mm was purchased from BioLogic. Concentrated H_2SO_4 (96.2%) was bought from Merck. All the experimental aqueous solutions were prepared in Milli-Q ultrapure water. The buffer solution (pH~7.4) was made by dissolving one commercial tablet of PBS in 200 mL water.

2.2. Fabrication of gold microelectrodes

The fabrication of gold microelectrodes of different sizes was performed by sealing hard gold fibers in Pasteur pipette. Before the sealing, the pipettes were cleaned in piranha solution and were dried overnight in an oven maintained at 110°C. A small length (ca. 1 cm) of fiber was cut and inserted in the narrow end of the pipette, which was subsequently sealed by placing Araldite glue (Araldite® 2011, Huntsman). The pipette was left in an upright position for 24 hours at room temperature for hardening of the glue. Following this, the tip of the pipette was polished using P600 Blackstone waterproof sandpaper to make the surface uniform and flat. The electrical connection with the fiber was established by filling the pipette with carbon powder and inserting a copper wire from the wide end of the pipette. Eventually, the microelectrodes were characterized by recording a CV in 0.1 M KCl aqueous solution containing 5 mM $K_3[Fe(CN)_6]$.

2.3. Electrochemical setup

All the electrochemical measurements were realized on a PGSTAT-320N Autolab potentiostat from Metrohm, which was connected with Nova 1.12 software. The experiments were performed using a conventional three-electrode cell consisting of NPG-deposited gold, Ag/AgCl (KCl sat.) and platinum as working, reference and counter electrodes, respectively. Before any electrochemical experiments, the gold electrode surface was cleaned by polishing over sandpaper having slurry of 0.05 µm alumina particles, followed by electrochemical cleaning under repetitive CV cycling in 0.5 M H_2SO_4 in the range of 0 to 1.6 V at a scan rate of 50 mV s^{-1}. The electrochemical studies for AA were performed by CV in a deoxygenated and neutral 0.1 M PBS solution, in the concentration range of 50–1000 µM and in the scan rate range of 5–1000 mV s^{-1}. All potential values reported in the manuscript are with reference to Ag/AgCl (KCl sat.).

2.4. Electrodeposition of NPG and electrochemical characterization

The electrodeposition of NPG on different Au microelectrodes and conventional Au disc electrodes was performed by chronoamperometry (at a fixed applied potential (E_d)) for a variable deposition time (t_d) in 5 mM $HAuCl_4$ + 0.5 M H_2SO_4 solution. The solution was strongly stirred to avoid formation of large H_2 bubbles on the Au electrode surface during the electrodeposition. Two sets of NPG films were electrodeposited on each gold electrode. In one group, NPG films at E_d = -1 V, -2 V, -3 V and -4 V were prepared for t_d = 100 s. In the other group, NPG films at E_d = -4 V were prepared for t_d = 100 s, 200 s, 400 s and 600 s. After the electrodeposition, NPG films were washed in distilled water. All electrodepositions were performed in the absence of any external gas bubbling and at room temperature. Following the electrodeposition, a CV of the NPG modified Au electrode was recorded in 0.5 M H_2SO_4 solution in the range of 0.2–1.6 V at a scan rate of 50 mV s^{-1}.

2.5. Morphology and surface characterizations

The SEM imaging was performed on a Scanning Electron Microscope (Quanta FEG 650), which was operated at accelerating voltage in the range of 3–20 kV. Images were recorded in horizontal scan of the surface. For the SEM imaging, the NPG deposited microelectrodes were cut from the narrow end of the pipette and placed on the substrate holder of the microscope. The electrical contact was established through a conducting carbon paste. During SEM imaging, EDS spectra and elemental mapping of NPG films were also conducted. Elemental and chemical purity analyses of the electrodeposited NPG films on Au substrate were performed on a Versaprobe 5000 XPS spectrometer (ULVAC-PHI apparatus). A monochromatic Al Kα X-ray source (1486.6 eV) was used during the measurements. In this characterization, survey and core-level spectra were recorded over a spot size of 200 µm. The spectra were further analyzed with XPS CASA software to estimate the elemental composition and deconvolution of the peaks.

3. Results and discussions

3.1. Electrochemical, morphologies and surface characterizations

The simplest way for a rapid and reliable characterization of NPG formation on the gold electrode is to record a CV in 0.5 M H_2SO_4 and compare it with the CV of bare gold electrode. Thus, Fig. 1a and 1b depict the comparisons of voltammograms of NPG prepared on 1.6 mm size gold disc electrode at different E_d for a fixed t_d and *vice versa*, respectively. The voltammograms of NPG coated Au electrodes are characterized by three oxidation waves in the range of 1.19 V to 1.45 V, which are attributed to the oxidation of gold into gold oxide at different crystalline faces of gold exposed to the solution interface [38, 39]. On the other hand, voltammogram of bare gold electrode (inset of Fig. 1b) shows only one oxidation wave, corresponding to the oxidation of gold into gold oxide at thermodynamically stable (111) facet of gold. Evolution of additional low-index crystalline faces is a characteristic feature of NPG film formation, which is assigned to the fast kinetics of gold atoms arrival at the nucleation center than the rate of crystallization during the deposition process [40, 41]. The cathodic scan of the voltammograms reveals a large reduction wave, which is associated to the reduction of gold oxide, formed in the forward scan, into gold. Notably, a large increase in the reduction current in the NPG voltammograms is evident, compared to the bare gold electrode CV, which is linked to the higher electrochemical surface area (ECSA) of the NPG surface because of its nanostructuration. Moreover, the increase in reduction peak current, is larger in the NPG films prepared by increasing t_d at a fixed E_d than increasing E_d at a fixed t_d, from the bare gold CV. It indicates increasing t_d is a more efficient way to enlarge NPG area than increasing E_d.

To get further insight into the variations of ECSA of NPG with the electrodeposition parameters E_d and t_d, similar NPG films were prepared on different sizes of Au microelectrodes

and their area was computed by the integration of the reduction peak of the CV. The detail of the calculation is given in the supporting information (Fig. S1). The variations of ECSA of the NPG films coated on different size Au electrodes, as a function of E_d and t_d are shown in Fig. 1c and 1d. From the ECSA evolution profiles of NPG, it is evident that NPG area increases linearly with more negative E_d, while an exponential increase is noticed with longer t_d. Moreover, the rate of area increase of NPG is faster when electrodeposited on gold disc electrode of size 1.6 mm, compared to the Au microelectrodes. Such a strong effect of the electrode substrate size and the electrodeposition parameters on the area evolution of the NPG is attributed to the different mass transport phenomena and kinetics of H_2 evolution, operating during the electrodeposition. Accordingly, surface morphologies of the NPG are expected to change with changing E_d and t_d as well as with Au electrode size.

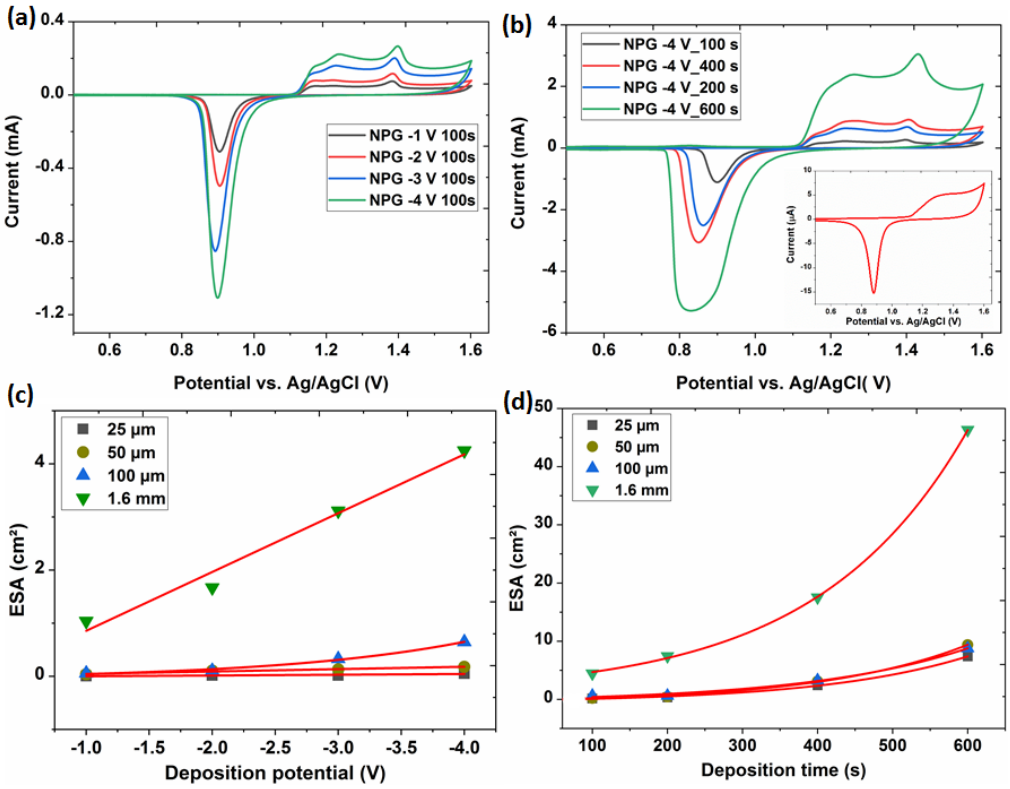

Figure 1: *Voltammograms of NPG modified Au electrodes prepared at different E_d (-1 V, -2 V, -3 V and -4 V) for a fixed t_d of 100 s (a) and at different t_d (100 s, 200 s, 400 s and 600 s) for a fixed E_d of -4 V (b), recorded in the range of 0.2–1.6 V at a scan rate of 50 mV s^{-1} in 0.5 M*

H_2SO_4 solution. CV obtained on bare Au electrode is given in the inset of (b). Variation of area of NPG film deposited on different sizes of Au electrodes (25 µm, 50 µm, 100 µm and 1.6 mm) with the change of E_d in the range of -1 V to -4 V (c) and t_d from 100 s to 600 s (d).

The surface morphologies of NPG films prepared at different E_d and t_d, over four different sizes of Au electrodes were studied by SEM imaging. The SEM images of the NPG surfaces are depicted in Fig. 2, exhibiting diverse morphological features, which depend on the electrodeposition parameters and the substrate size. The upper panel in Fig. 2 shows the images of NPG prepared at low E_d = -1 V and short t_d = 100 s on four different sizes Au electrodes. The morphology of the NPG prepared on 25 µm Au electrode reveals a partial honeycomb structure, such that a part of the surface has deep macropores, while a fraction of the surface lacks the complete growth of the macropores and the walls surrounding them. On the other hand, the morphologies of the NPG prepared under the similar electrodeposition conditions on the larger size Au electrodes lack honeycomb features and are rather compact. In particular, the NPG film prepared on 1.6 mm Au electrode contains homogeneously distributed aggregates of gold nanocrystals and is devoid of µm-size surface pores. Nonetheless, these compact NPG surfaces have nanometer size pores as evidenced in the magnified SEM images (Fig. S2).

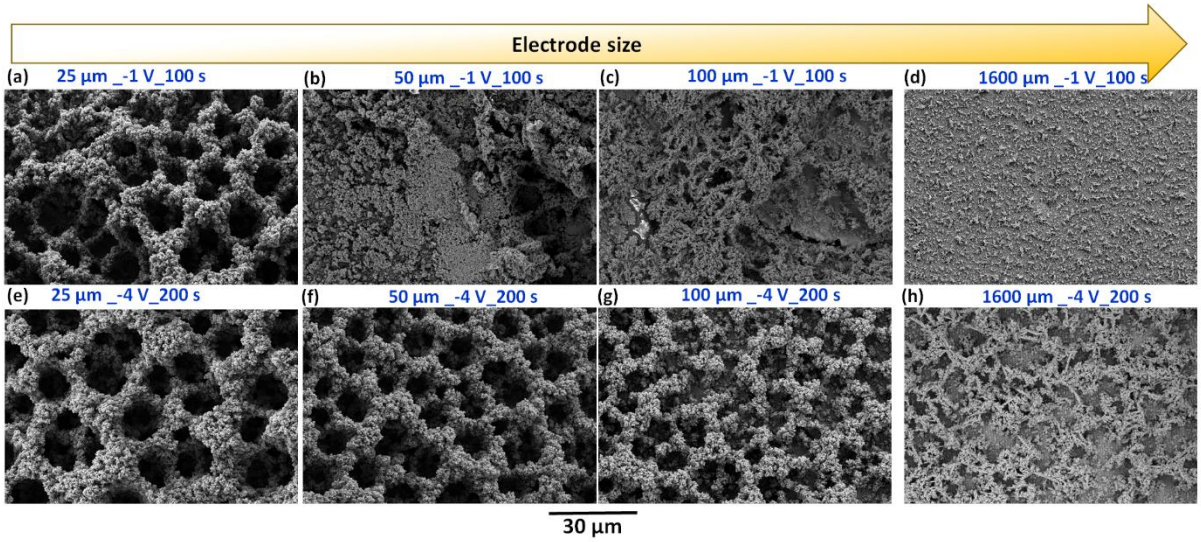

Figure 2*: SEM images of NPG films prepared at E_d = -1 V and t_d = 100 s (a, b, c and d) and E_d = -4 V and t_d = 200 s (e, f, g and h), coated on different sizes of Au electrodes.*

The change in the NPG surface morphology, deposited on the same set of Au electrodes at more negative E_d (-4 V) and for longer t_d (200 s) are shown in the lower image panels in Fig. 2. From the SEM images, it is evident that electrodeposition on smaller size Au substrates (25 µm and 50 µm) results in the growth of NPG films with well-defined honeycomb structure, while on the larger Au substrates, deposited NPG films possess partial honeycomb feature. Indeed, the morphology of the NPG prepared on 25 µm Au electrode reveals hierarchically distributed and interconnected macropores, such that pores at the surface are bigger in size and become smaller in the inner volume. This feature is attributed to the coalescence of H_2 bubbles with the progress of the electrodeposition, imparting a larger size template for the pores evolution in the gold deposit. It is also observed that surface pores decrease in size and the walls surrounding the pores become thinner, for the NPG prepared at more negative E_d and longer t_d, with the increase of the Au substrate diameter. Such wide variations in the morphologies of the NPG with changing substrate size can be assigned to the different mass transport during the electrodeposition. The mass transport would be more vigorous with the decreasing size of Au electrodes, owing to the increasing radial diffusion, which provides larger flux of mass (H^+ and Au^{3+}) to the electrode. Thus, H_2 evolution reaction and Au^{3+} reduction would be faster on 25 µm size electrode, generating macropores and thicker wall in the NPG film. The change of compact surface of NPG into porous surface by making E_d more negative and t_d longer, at larger Au substrates is explained by the fastening of the rate of H_2 evolution and Au^{3+} reduction reaction at higher cathodic potential. Thus, it would result in the generation of more H_2 bubbles and larger Au deposit. At longer t_d, the smaller H_2 bubbles coalesce into larger bubbles, consequently inducing larger pores in the gold deposit. The NPG films were few µm thick and contained micropores within the cross-section (Fig. S3).

Besides honeycomb feature of the NPG surfaces at the micrometric scale, the interconnected wall forming the macropores, are highly porous at the nanometric scale (Fig. 3a). The nanometric structure of the NPG takes the form of highly branched dendrite fractals, which is a typical feature of diffusion limited aggregation growth model of metal deposition [42] and has been previous reported for NPG surfaces [39]. The dendrites contain a few hundred nm long trunks and few tens of nm long branches. The SEM image exhibits presence of multiplicity of nanopores on the NPG surface, which also justify the large ECSA of the films. Similar dendrite features and nanometric pores were also visualized in a higher resolution SEM image shown in Fig. S4. NPG films were characterized for their chemical purity, considering the risk of chloride contamination, while using $HAuCl_4$ as a precursor for the NPG deposition. The bulk chemical purity of the NPG surface over a large micrometric area was assessed by performing EDS mapping over a large micrometric area. The sum of the EDS spectra over the mapped region exhibited mainly gold peaks, confirming the high purity of the NPG films (Fig. S5). The presence of small quantity of carbon is because of the use of carbon paste to establish electrical contact between sample and the substrate holder of SEM microscope. Beside bulk elemental analysis, surface elemental composition of the NPG film was also characterized by XPS. The survey spectrum of NPG surface (Fig. S6) reveals the peaks mainly associated to gold, further confirming the high surface purity of the prepared NPG films. The spectrum is devoid of a peak associated to metal chloride (~198.5–199 eV). Thus the surface contamination of the NPG from chloride during the electrodeposition is ruled out. Chemical purity of the NPG film was also examined by recording core-level XPS spectra (Fig. 3b), exhibiting the characteristic peaks associated to Au $4f_{5/2}$ and Au $4f_{7/2}$ subshells at 87.6 eV and 84.1 eV, respectively [43]. These peak positions of Au are consistent with its metallic form and rules out any charge transfer to form a bond with heteroatoms.

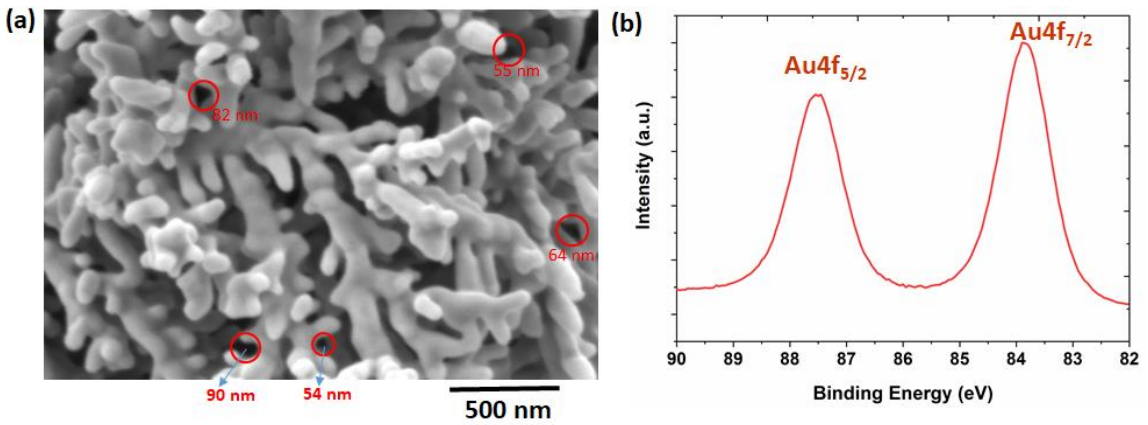

Figure 3: *SEM image (a) and XPS spectrum (b) of NPG film prepared at E_d = -4 V and t_d = 200 s on 1.6 mm Au electrode.*

3.2. Electrochemical process of AA on NPG

Electrochemical activity of NPG electrodeposited at different E_d and t_d over the set of four Au electrodes was investigated towards AA oxidation process by CV in a wide scan rate and AA concentration ranges. Comparison of the voltammograms recorded in the presence of 0.6 mM AA and in its absence in 0.1 M PBS solution are shown in Fig. 4 for NPG deposited on 25 µm and 1.6 mm Au electrodes, while similar CVs for NPG deposited on 50 µm and 100 µm Au electrodes are shown in Fig. S5. The CVs recorded in the presence of AA depict a sharp oxidation wave, typical for a fast electron transfer kinetics, in the anodic scan at all the NPG electrodes, which is associated to the irreversible oxidation of AA into DHA. The oxidation wave observed at different NPG electrodes either forms a peak around Ep ca. 0 V or presents a steady state sigmoidal curve with $E_{1/2} < 0$ V. On the other hand, bare gold electrodes show a less steep rise of the AA oxidation wave, typical for slower electron transfer kinetics, peaking at 0.35 V on 1.6 mm Au electrode (inset of Fig. 4d) and non-steady state increasing profile on 25 µm Au electrodes (inset of Fig. 4a). From the shift of AA oxidation Ep by more than 350 mV towards zero, sharper oxidation wave and larger oxidation peak current (ip) on NPG electrodes, compared to bare Au electrodes, it is evident that AA electrochemical process is electrocatalysed on the NPG electrodes. However, the shape of the AA oxidation wave changes, depending on E_d and t_d of NPG deposition and on the size of the Au electrode. For instance,

oxidation wave is sigmoidal on NPG deposited at E_d = -1 V and t_d = 100 s on 25 µm Au electrode (Fig. 4a), comprising a sharp increase of current followed by a steady-state condition during the remaining anodic scan. Such voltammetric profile is typical for microelectrode, owing to the dominance of radial diffusion for the mass transfer at the electrode surface. The shape of the AA oxidation wave changes from sigmodal shape to non-symmetric peak form with a broad peak, on the NPG prepared at more negative E_d (-4 V) (Fig. 4b) and for longer t_d (600 s) (Fig. 4c) on 25 µm Au electrode. Such peak shapes predict that mass transport of AA is governed by planar diffusion. The variation of the shape of AA oxidation wave follows different trends on the NPG prepared on 1.6 mm Au electrode. The oxidation wave has a broad and non-symmetric peak on the NPG prepared at E_d = -1 V and for t_d = 100 s, indicating a planar diffusion of AA. However, the peak of the oxidation wave becomes sharper and more symmetric on the NPG prepared at more negative E_d and for longer t_d. Indeed, a highly symmetrical oxidation peak of AA is noticed in Fig. 4f on NPG prepared at E_d = -4 V and t_d = 600 s. Such shape is a characteristic feature of adsorption or confined (thin layer diffusion) process during AA redox mechanism [44]. The appearance of large capacitive current in the CV is accounted to the huge enlargement of NPG area at longer deposition time. The AA oxidation wave experiences similar transition in its shape on the NPG prepared on 100 µm Au electrodes (Fig. S7). On the other hand, oxidation wave of AA on NPG prepared at 50 µm Au electrode changes from a sigmoidal shape to a non-symmetric peak by making E_d more negative and to a symmetrical peak at longer t_d (Fig. S7) Thus, it is clear that mass transport of AA and its redox mechanism depend on the electrodeposition parameters (E_d and t_d) of NPG and the size of the substrate Au electrode.

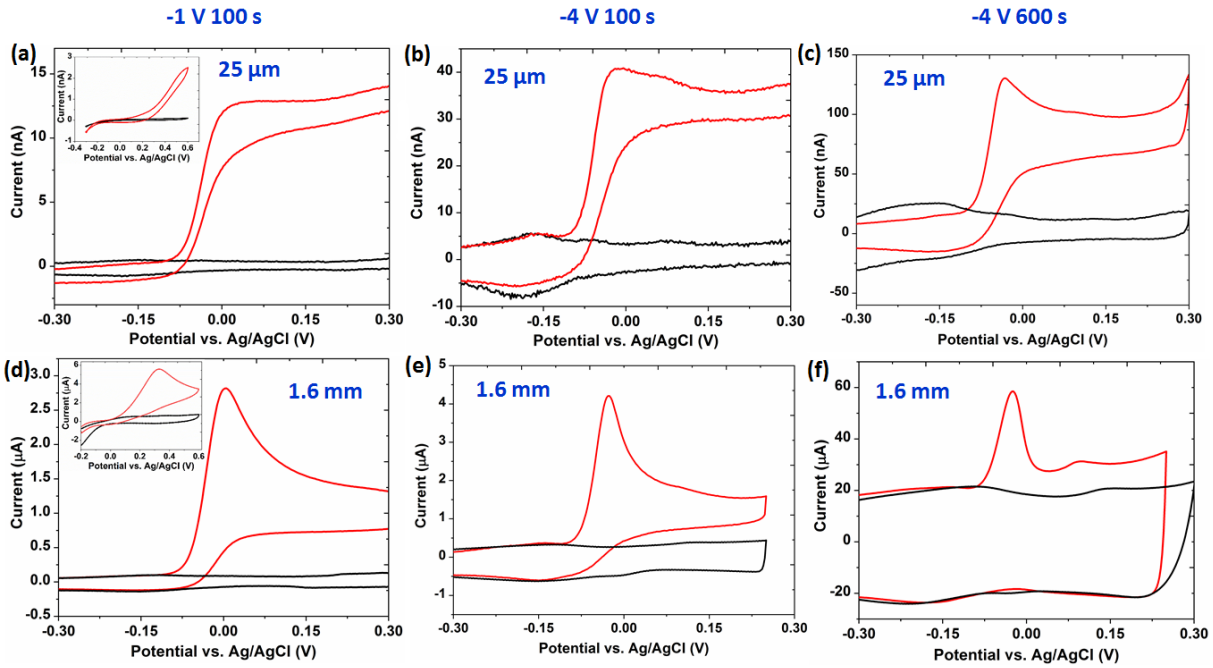

Figure 4: *Comparison of cyclic voltammograms, recorded in 0.6 mM AA + 0.1 M PBS and 0.1 M PBS solutions on NPG prepared at E_d = -1 V and t_d = 100 s (a and d), E_d = -4 V and t_d = 100 s (b and e) and E_d = -4 V and t_d = 600 s (c and f) on 25 µm and 1.6 mm diameter Au electrodes. Scan rate: 10 mV s^{-1}. The CV obtained on bare gold microelectrode of 25 µm size and on 1.6 mm size Au electrode are given in the inset of (a) and (d), respectively.*

Chronoamperometry (CA) test provides a direct experimental evidence of thin layer diffusion as reported previously [45]. We performed such studies on the bare gold and NPG modified gold electrode in AA concentration range of 0.5 mM to 4 mM. The experimentally observed CA curves on the bare gold and the NPG coated Au electrode are shown in Fig. 5a and 5b, respectively. Notably, the current decay profiles corresponding to AA electrooxidation are relatively slower on the bare Au electrode than on the NPG modified Au electrode. The time taken by the CA curves to become asymptotic with respect to x-axis and stay steady-state thereafter on bare Au electrode, is than 40 s. On the other hand, the similar change in the CA curves current values on the NPG modified Au electrode takes less than 3 s. It confirms that electron transfer process is very rapid in NPG modified Au electrode, which can be associated

to a small diffusion length available for AA trapped within the porous volume of NPG. Such confined environment enhances the collision frequency of AA with the electrified wall of the NPG, resulting in the faster electron transfer rate [46]. Such diffusion regime can be categorized as thin layer diffusion. Moreover, the magnitude of the maximum current at the onset of the CA curves are more than 10 times higher on the NPG modified Au electrode than on the bare Au electrode. This is assigned to the large available electroactive area in NPG modified Au electrode because of the nanostructuration. The CA curves at 3 mM AA concentration on the both the electrodes were further assessed through comparing their Cottrell plots as shown in Fig. 5c. It is evident from the figure that in NPG modified Au electrode, the current curve versus $t^{-1/2}$ has two slopes, in which the one at shorter time is much larger than the one at the longer time. The presence of two slopes provides a direct evidence of thin layer diffusion in NPG modified Au electrode [45]. The region of the curve at shorter time is called Cottrell region and originates from the thin layer diffusion of the AA trapped within the NPG volume. Notably, the small amount of the AA trapped inside the NPG volume is quickly depleted, diminishing the mass transfer to the electrified electrode, thus causing decrease in the slope values at longer time. However, the slope value at longer times never becomes zero because there is always a small flux of AA mass arriving from the bulk solution to the outer surface of the NPG electrode. The Cottrell plot of bare Au electrode presents only one slope, attesting the presence of only one diffusion regime, which is from the bulk solution.

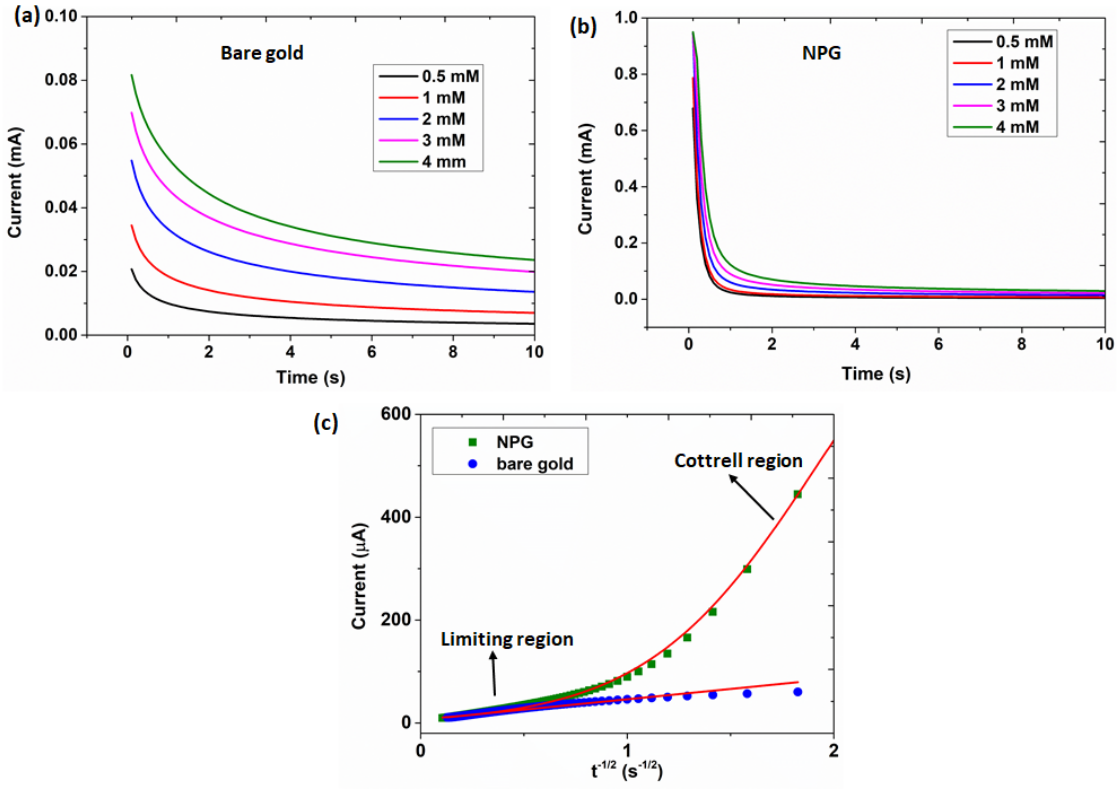

Figure 5: chronoamperogram of AA at different concentrations on bare Au (a) and NPG modified Au electrode (b). Comparison of the Cottrell plots of the associated CA curves at 3 mM AA on the two electrodes (c).

3.3. Redox mechanism and mass transport of AA on NPG

The redox mechanism of AA, as reported previously, involves coupled reactions, in which AA is at first electrochemically (E) oxidized into DHA through exchange of $2e^-$ and $2H^+$, followed by hydration of DHA through a fast 1st order chemical reaction (C_1) [17]. Thus, such mechanism is termed as EC_1. The electrochemical step can involve different diffusional mass transport as well as adsorption of AA. Notably, there are two different diffusion regimes of electroactive analyte on porous electrode as reported previously [47, 48]. Accordingly, AA in the bulk solution diffuses to the surface of NPG and AA present in the trapped electrolytic solution inside the volume of NPG electrode undergoes thin layer diffusion through the

interconnect struts of NPG. In thin layer diffusion regime, AA experiences rapid oxidation and thus its depletion within the NPG volume due to the shorter path length and possibility of multiple collisions with the porous walls of the electrode. Nonetheless, the relative contribution of bulk diffusion and thin layer diffusion is determined by the thickness of the porous layer and the sizes of the pores. Accordingly, the oxidation process of AA is named as diffusion EC_1 and thin layer EC_1, depending on the predominance of AA diffusion from bulk solution and AA diffusion and adsorption within the porous volume, respectively. The nature of the followed chemical reaction can be homogeneous (in bulk and trapped solution inside NPG volume) or heterogeneous (on surface). Based on these hypotheses, the redox mechanism of AA can be rationalized through a square scheme as depicted in Fig. 6 on NPG deposited on different sizes Au electrodes. The scheme commences with the diffusion of AA from the bulk solution to the NPG outer surface-solution interface, where it can either undergo reversible electrochemical oxidation into DHA or enter into the NPG porous volume to further enrich AA already trapped inside. The predominance of the either event depends on the porous morphologies of the NPG, such that a flat surface would favour the former event, while a highly porous surface would significantly experience the latter phenomenon. Moreover, the nature of the Au crystalline facets exposed to the electrode-solution interface plays a significant role in the adsorption phenomenon, which evolution into an NPG microstructure is determined by the choice of E_d and t_d, as reported in our previous work [28].

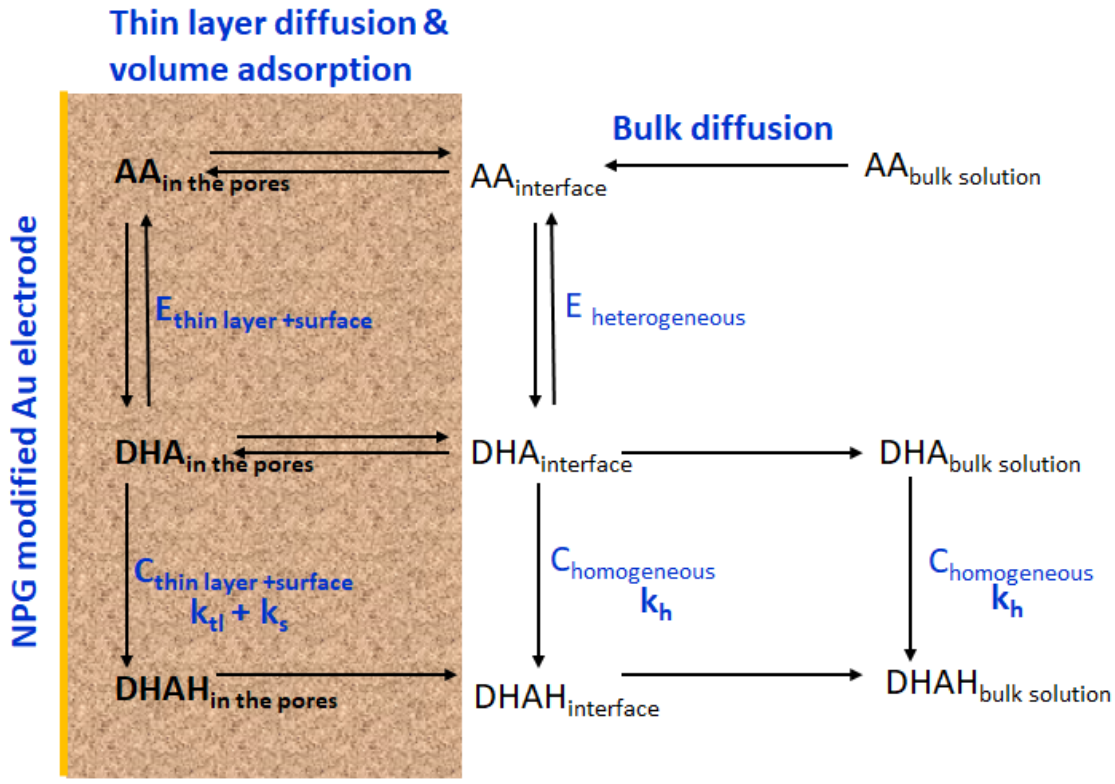

Figure 6 *The reaction scheme of AA oxidation processes on NPG modified gold electrodes*

The DHA formed at the electrode-solution interface can either diffuse back into the bulk solution or it can undergo a hydration, forming DHAH through a homogeneous chemical reaction in the solution, which is finally transported away in the bulk solution. In the situation where AA is confined in the pores, it can undergo thin layer diffusion and adsorption on the porous wall of NPG, resulting in a reversible electrochemical reaction to form DHA. The DHA so formed can either remain into the pores or can arrive in the solution near the NPG-bulk solution interface. In the latter case, the DHA will undergo a homogeneous irreversible chemical reaction forming DHAH and finally would go in the bulk solution. In the former case, the DHA remaining in the pores will be hydrated into DHAH through an irreversible confined reaction, which would subsequently pass into the bulk solution through the electrode-bulk solution interface.

Although, the square scheme predicted different redox pathways of AA, the preferred redox pathways depend on the porous geometry of NPG and thus the associated mass transport. Figure 7 depicts schematic representation of diffusion layers formed in two different porous geometries of NPG. In the thicker NPG film, pores grow in size hierarchically in the direction of away from the substrate surface. Moreover, pores are interconnected, as also evidenced in the SEM images. Consequently, the cross-section of the diffusion layer so formed contains the stacked circular zones, which are growing in diameter in the direction away from the substrate and are interconnected to each other (Fig. 7a). In such diffusion layer configuration, thin layer diffusion is dominant deeper inside the volume, where pores are smaller, causing a rapid depletion of AA and accumulation of DHA. On the other hand, in the NPG volume cross-section near the surface of the film, where pores are bigger in size, thin layer diffusion is limited, as arrival of AA flux from the bulk solution dominates and larger pores facilitate the removal of DHA into the bulk solution. The extent of AA adsorption in such porous volume of NPG depends on crystalline structural properties of gold (lattice orientation and defects) [24, 28] and the sizes of the surface pores. Accordingly, smaller pores would favour multiple collision of AA with NPG struts and thus provide higher probability of confined reactions, while larger pores will favour enhanced diffusion of AA from the bulk solution. In the other scenario, where pores are not yet evolved but the NPG film contains a rough surface because of deposition of Au nanocrystals at different nucleation sites, the formation of diffusion layer is shown in Fig. 7b. In such morphology, a hemispherical diffusion layer is formed around each nanocrystal aggregate upon electrode polarization. The merging of the individual spherical layer forms a plane, which typically behaves as a planar diffusion layer as reported previously [49, 50]. Thus the mass transport mainly involves the bulk diffusion of AA.

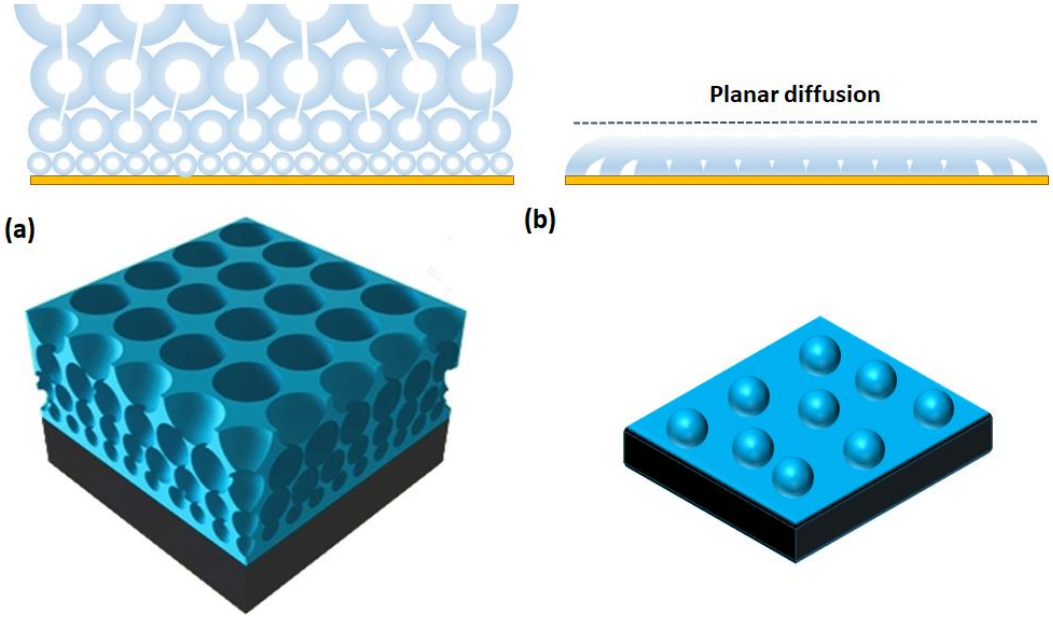

Figure 7: *Schematic representation diffusion layer formed in thick NPG film and thin NPG film modified electrode.*

The aforementioned models of the mass transport and redox mechanism of AA can be correlated to the evolution of the voltammetric profiles of AA on NPG modified Au electrodes of different size (Fig. 4). Thus, shape of a AA oxidation wave is determined by the interplay of bulk diffusion, thin layer diffusion and adsorption, which relative contribution is determined by the morphology of the NPG films. NPG films coated on 25 µm size Au electrode has larger surface pores irrespective of the deposition conditions (E_d and t_d), which facilitates significant transfer of AA mass from the bulk solution. Moreover, spherical shape of the diffusion layer and interconnection within the volume provides a continuous flux of AA and removal of DHA. Consequently, the voltammetric profiles of AA on these electrodes feature a sigmodal or a broad peak shape. Notably, the non-symmetric peak of AA oxidation on NPG prepared at longer t_d = 600 s is attributed to higher thin layer diffusion contribution because of larger film thickness. Moreover, NPG film prepared at longer t_d contains higher concentration of low-indexed Au plane, where AA displays stronger adsorption. The diffusion regimes in the NPG

modified 1.6 mm Au electrode at E_d = -1 V and t_d = 100 s are dominated by planar diffusion, because, it lacks well-defined surface pores (Fig. 2d). Thus, it explains the appearance of a non-symmetric peak of AA oxidation wave. On increasing the E_d and t_d of NPG deposition on 1.6 mm Au electrode (Fig. 2h), the morphologies become porous with the presence of smaller pores and rich in low-indexed Au planes. Therefore, the relative contributions of thin layer diffusion (and adsorption) rise, which make the voltammetric peak of AA oxidation more symmetric.

Conclusions

In summary, the mass transport associated to AA oxidation process has been explored on NPG surfaces, which demonstrated strong dependence on the electrodeposition parameters of the NPG synthesis and the size of the Au substrate. The NPG prepared by template-assisted potentiostatic electrodeposition reveals high chemical purity and huge enhancement in the surface area compared to the bare Au electrode. The surface morphology of NPG exhibits diverse features, depending on the electrodeposition conditions, E_d and t_d, as well as the size of the Au substrate. Accordingly, the surface becomes more porous, exhibiting a well-defined honeycomb structure, by increasing the cathodic deposition potential and the deposition time of NPG synthesis. Moreover, the size of the surface pores increases by decreasing the diameter of the substrate Au electrode at the same electrodeposition conditions (E_d and t_d). The AA oxidation process shows different voltammetric profiles with changing substrate size and electrodeposition parameters (E_d and t_d) of NPG synthesis. The voltammetric feature obtained at NPG prepared on smaller size Au microelectrodes is sigmoidal or non-symmetric peak, which is attributed to the larger sizes of the surface pores. Such morphologies allow an easier transport of AA from the bulk solution and removal of DHA from the NPG volume. On the other hand, NPG prepared on larger size Au electrode display non-symmetric peak at less

negative E_d and shorter t_d, which changes into symmetric peak on NPG prepared at more negative E_d and longer t_d. Such transition is attributed to the increasing contribution of thin layer diffusion and adsorption in the NPG film, which are further correlated to the smaller surface pores and reactive crystalline facets of Au, obtained at more negative E_d and longer t_d.

Acknowledgments

Authors are thankful for receiving financial grant from European Union through PO FEDER-FSE Bourgogne 2019/2022 (via CoMICS program), Agence Nationale de la Recherche (ANR) (OUTSMART ANR-2015-CE39-0004-03) and Conseil Régional de Bourgogne (CPER program). A.K. acknowledges fellowship from BQR program and MatElectroCap project. Authors also thanks O. Heintz and A. Krystianiak for performing XPS measurements.

References

[1] J.M. Gonçalves, A. Kumar, M.I. da Silva, H.E. Toma, P.R. Martins, K. Araki, M. Bertotti, L. Angnes, Nanoporous gold-based materials for electrochemical energy storage and conversion, Energy Technol. 9 (2021) 2000927.

[2] H.J. Qiu, H.-T. Xu, L. Liu, Y. Wang, Correlation of the structure and applications of dealloyed nanoporous metals in catalysis and energy conversion/storage, Nanoscale, 7 (2015) 386-400.

[3] W. Luc, F. Jiao, Nanoporous Metals as Electrocatalysts: State-of-the-Art, opportunities, and challenges, ACS Catal. 7 (2017) 5856-5861.

[4] Y. Pei, M. Hu, F. Tu, X. Tang, W. Huang, S. Chen, Z. Li, Y. Xia, Ultra-rapid fabrication of highly surface-roughened nanoporous gold film from AuSn alloy with improved performance for nonenzymatic glucose sensing, Biosens. Bioelectron. 117 (2018) 758-765.

[5] X. Ke, Z. Li, L. Gan, J. Zhao, G. Cui, W. Kellogg, D. Matera, D. Higgins, G. Wu, Three-dimensional nanoporous Au films as high-efficiency enzyme-free electrochemical sensors, Electrochim. Acta, 170 (2015) 337-342.

[6] C. Xu, F. Sun, H. Gao, J. Wang, Nanoporous platinum–cobalt alloy for electrochemical sensing for ethanol, hydrogen peroxide, and glucose, Anal. Chim. Acta, 780 (2013) 20-27.

[7] Y. Mie, H. Takayama, Y. Hirano, Facile control of surface crystallographic orientation of anodized nanoporous gold catalyst and its application for highly efficient hydrogen evolution reaction, J. Catal. 389 (2020) 476-482.

[8] Y. Peng, T. Wu, L. Sun, J.M.V. Nsanzimana, A.C. Fisher, X. Wang, Selective electrochemical reduction of CO_2 to ethylene on nanopores-modified copper electrodes in aqueous solution, ACS Appl. Mater. Interfaces, 9 (2017) 32782-32789.

[9] J.-H. Han, E. Lee, S. Park, R. Chang, T.D. Chung, Effect of Nanoporous structure on enhanced electrochemical reaction, J. Phys. Chem. C, 114 (2010) 9546-9553.

[10] J.H. Bae, J.-H. Han, D. Han, T.D. Chung, Effects of adsorption and confinement on nanoporous electrochemistry, Faraday Discuss. 164 (2013) 361-376.

[11] S. Faucher, N. Aluru, M.Z. Bazant, D. Blankschtein, A.H. Brozena, J. Cumings, J. Pedro de Souza, M. Elimelech, R. Epsztein, et al., Critical knowledge gaps in mass transport through single-digit nanopores: A review and perspective, J. Phys. Chem. C, 123 (2019) 21309-21326.

[12] D.A. McCurry, R.C. Bailey, Nanoporous gold membranes as robust constructs for selectively tunable chemical transport, J. Phys. Chem. C, 120 (2016) 20929-20935.

[13] Y. Ding, Y.J. Kim, J. Erlebacher, Nanoporous Gold Leaf: "Ancient technology"/advanced material, Adv. Mater. 16 (2004) 1897-1900.

[14] A. El Mel, F. Boukli-Hacene, L. Molina-Luna, N. Bouts, A. Chauvin, D. Thiry, E. Gautron, N. Gautier, P.-Y. Tessier, Unusual dealloying effect in gold/copper alloy thin films: the role of defects and column boundaries in the formation of nanoporous gold, ACS Appl. Mater. Interfaces, 7 (2015) 2310-2321.

[15] C. Li, M. Iqbal, J. Lin, X. Luo, B. Jiang, V. Malgras, K.C.W. Wu, J. Kim, Y. Yamauchi, Electrochemical deposition: An advanced approach for templated synthesis of nanoporous metal architectures, Acc. Chem. Res., 51 (2018) 1764-1773.

[16] B.J. Plowman, L.A. Jones, S.K. Bhargava, Building with bubbles: the formation of high surface area honeycomb-like films via hydrogen bubble templated electrodeposition, Chem. Commun. 51 (2015) 4331-4346.

[17] F. Prieto, B.A. Coles, R.G. Compton, Mechanistic determination using arrays of variable-sized channel microband electrodes: The oxidation of ascorbic acid in aqueous solution, J. Phys. Chem. B, 102 (1998) 7442-7447.

[18] A.M. Pisoschi, A. Pop, A.I. Serban, C. Fafaneata, Electrochemical methods for ascorbic acid determination, Electrochim. Acta, 121 (2014) 443-460.

[19] N. Smirnoff, Ascorbic acid metabolism and functions: A comparison of plants and mammals, Free Radical Biol. Med. 122 (2018) 116-129.

[20] S. Li, G. Chen, C. Zhang, M. Wu, S. Wu, Q. Liu, Research progress of natural antioxidants in foods for the treatment of diseases, Food Sci. Hum. Wellness, 3 (2014) 110-116.

[21] M. Rueda, A. Aldaz, F. Sanchez-Burgos, Oxidation of L-ascorbic acid on a gold electrode, Electrochim. Acta, 23 (1978) 419-424.

[22] J. Wang, B.A. Freiha, Evaluation of differential pulse voltammetry at carbon electrodes, Talanta, 30 (1983) 317-322.

[23] K. Dhara, R.M. Debiprosad, Review on nanomaterials-enabled electrochemical sensors for ascorbic acid detection, Anal. Biochem. 586 (2019) 113415.

[24] S.K. De, S. Mondal, P. Sen, U. Pal, B. Pathak, K.S. Rawat, M. Bardhan, M. Bhattacharya, B. Satpati, A. De, D. Senapati, Crystal-defect-induced facet-dependent electrocatalytic activity of 3D gold nanoflowers for the selective nanomolar detection of ascorbic acid, Nanoscale, 10 (2018) 11091-11102.

[25] L. Zhang, F. Liu, X. Sun, G.-f. Wei, Y. Tian, Z.-P. Liu, R. Huang, Y. Yu, H. Peng, Engineering carbon nanotube fiber for real-time quantification of ascorbic acid levels in a live rat model of alzheimer's disease, Anal. Chem. 89 (2017) 1831-1837.

[26] A. Kumar, V.L. Furtado, J.M. Gonçalves, R. Bannitz-Fernandes, L.E.S. Netto, K. Araki, M. Bertotti, Amperometric microsensor based on nanoporous gold for ascorbic acid detection in highly acidic biological extracts, Anal. Chim. Acta, 1095 (2020) 61-70.

[27] A. Kumar, J.S.G. Selva, J.M. Gonçalves, K. Araki, M. Bertotti, Nanoporous gold-based dopamine sensor with sensitivity boosted by interferant ascorbic acid, Electrochim. Acta, 322 (2019) 134772.

[28] A. Kumar, J.M. Gonçalves, J.S.G. Selva, K. Araki, M. Bertotti, Correlating selective electrocatalysis of dopamine and ascorbic acid electrooxidation at nanoporous gold surfaces with structural-defects, J. Electrochem. Soc. 166 (2019) H704-H711.

[29] T.A. Silva, M.R.K. Khan, O. Fatibello-Filho, M.M. Collinson, Simultaneous electrochemical sensing of ascorbic acid and uric acid under biofouling conditions using nanoporous gold electrodes, J. Electroanal. Chem. 846 (2019) 113160.

[30] A.A. Farghaly, M. Lam, C.J. Freeman, B. Uppalapati, M.M. Collinson, Potentiometric measurements in biofouling solutions: Comparison of nanoporous gold to planar gold, J. Electrochem. Soc. 163 (2015) H3083-H3087.

[31] C.J. Freeman, B. Ullah, M.S. Islam, M.M. Collinson, Potentiometric biosensing of ascorbic acid, uric acid, and cysteine in microliter volumes using miniaturized nanoporous gold electrodes, Biosens. 11 (2021) 10.

[32] D. Zhao, D. Fan, J. Wang, C. Xu, Hierarchical nanoporous platinum-copper alloy for simultaneous electrochemical determination of ascorbic acid, dopamine and uric acid, Microchim. Acta, 182 (2015) 1345-1352.

[33] D. Zhao, G. Yu, K. Tian, C. Xu, A highly sensitive and stable electrochemical sensor for simultaneous detection towards ascorbic acid, dopamine, and uric acid based on the hierarchical nanoporous Pt-Ti alloy, Biosens. Bioelectron. 82 (2016) 119-126.

[34] H. Yang, J. Zhao, M. Qiu, P. Sun, D. Han, L. Niu, G. Cui, Hierarchical bi-continuous Pt decorated nanoporous Au-Sn alloy on carbon fiber paper for ascorbic acid, dopamine and uric acid simultaneous sensing, Biosens. Bioelectron. 124-125 (2019) 191-198.

[35] H. Boo, S. Park, B. Ku, Y. Kim, J.H. Park, H.C. Kim, T.D. Chung, Ionic strength-controlled virtual area of mesoporous platinum electrode, J. Am. Chem. Soc. 126 (2004) 4524-4525.

[36] J. Veselinovic, S. AlMashtoub, S. Nagella, E. Seker, Interplay of effective surface area, mass transport, and electrochemical features in nanoporous nucleic acid sensors, Anal. Chem. 92 (2020) 10751-10758.

[37] A. Kumar, J.M. Gonçalves, V.L. Furtado, K. Araki, L. Angnes, M. Bouvet, M. Bertotti, R. Meunier-Prest, Mass transport in nanoporous gold and correlation with surface pores for EC_1 mechanism: Case of ascorbic acid, ChemElectroChem, 8 (2021) 2129-2136.

[38] A. Hamelin, Cyclic voltammetry at gold single-crystal surfaces. Part 1. Behaviour at low-index faces, J. Electroanal. Chem. 407 (1996) 1-11.

[39] A. Kumar, J.M. Gonçalves, A. Sukeri, K. Araki, M. Bertotti, Correlating surface growth of nanoporous gold with electrodeposition parameters to optimize amperometric sensing of nitrite, Sens. Actuators, B, 263 (2018) 237-247.

[40] M.K. Khristosov, L. Bloch, M. Burghammer, Y. Kauffmann, A. Katsman, B. Pokroy, Sponge-like nanoporous single crystals of gold, Nat. Commun. 6 (2015) 8841.

[41] H.E.M. Hussein, R.J. Maurer, H. Amari, J.J.P. Peters, L. Meng, R. Beanland, M.E. Newton, J.V. Macpherson, Tracking metal electrodeposition dynamics from nucleation and growth of a single atom to a crystalline nanoparticle, ACS Nano, 12 (2018) 7388-7396.

[42] T.A. Witten, L.M. Sander, Diffusion-limited aggregation, a kinetic critical phenomenon, Phys. Rev. Lett. 47 (1981) 1400-1403.

[43] P. Jiang, S. Porsgaard, F. Borondics, M. Köber, A. Caballero, H. Bluhm, F. Besenbacher, M. Salmeron, Room-temperature reaction of oxygen with gold: An *in situ* ambient-pressure X-ray photoelectron spectroscopy investigation, J. Am. Chem. Soc. 132 (2010) 2858-2859.

[44] A. Kaliyaraj Selva Kumar, R.G. Compton, Understanding carbon nanotube voltammetry: distinguishing adsorptive and thin layer effects via “Single-Entity” electrochemistry, J. Phys. Chem. Lett. 13 (2022) 5557-5562.

[45] M. Liberatore, A. Petrocco, F. Caprioli, C. La Mesa, F. Decker, C.A. Bignozzi, Mass transport and charge transfer rates for Co(III)/Co(II) redox couple in a thin-layer cell, Electrochim. Acta, 55 (2010) 4025-4029.

[46] R.J. White and H.S. White, A Random Walk through Electron-Transfer Kinetics, Analytical Chemistry, 77 (2005) 214 A-220 A.

[47] E.O. Barnes, X. Chen, P. Li, R.G. Compton, Voltammetry at porous electrodes: A theoretical study, J. Electroanal. Chem. 720-721 (2014) 92-100.

[48] M.C. Henstridge, E.J.F. Dickinson, M. Aslanoglu, C. Batchelor-McAuley, R.G. Compton, Voltammetric selectivity conferred by the modification of electrodes using conductive porous layers or films: The oxidation of dopamine on glassy carbon electrodes modified with multiwalled carbon nanotubes, Sens. Actuators B: Chem. 145 (2010) 417-427.

[49] G. Gunawardena, G. Hills, I. Montenegro, B. Scharifker, Electrochemical nucleation: Part I. General considerations, J. Electroanal. Chem. Interfacial Electrochem. 138 (1982) 225-239.

[50] B. Scharifker, G. Hills, Theoretical and experimental studies of multiple nucleation, Electrochim. Acta, 28 (1983) 879-889.